Available online www.jsaer.com

Journal of Scientific and Engineering Research, 2021, 8(12):41-46

Research Article

ISSN: 2394-2630
CODEN(USA): JSERBR

Investigation of the tectonic structure of the Magnetic Anomaly Map of the Black Sea Region by Cellular Artificial Neural Network (CNN) Method

Ali Muhittin ALBORA

Istanbul University-Cerrahpaşa, Engineering Faculty, Geophysical Department, Büyükçekmece-Istanbul, Turkey
Email: muhittin@iucl.edu.tr

Abstract In this study, the structure boundaries were determined by applying the Cellular Neural Network (CNN) method to the magnetic anomaly map of the Black Sea. The Black Sea is one of the world's largest inland seas. As you move away from the shelf parts, the water depth decreases rapidly on average by 2 km. The Black Sea sediments are very rich in calcite and organic carbon, which indicates a high degree of conservation due to the anaerobic environment starting from a depth of 100-150 m. The general tectonic structure of the Black Sea and the surrounding region was compared with the boundaries of the structures. Thus, the tectonic structure of the region was tried to be clarified in the light of tectonic information with the CNN output of the magnetic anomaly map.

Keywords Black Sea, Mannetic anomaly, Cellular Neural Network (CNN)

Introduction

Cellular Artificial Neural Networks (CNN), a special type of artificial neural networks, were first introduced in 1988 by Leon Chua and Lin Yang [1]. Two-dimensional structures have found widespread use in image processing [2-6] and their locations were tried to be determined [7-8]. In geophysical engineering, CNN method yielded much more successful results than classical methods in separating potential field anomalies from regional and residual anomalies [9-10]. In this study, the Cellular Artificial Neural Network (CNN) method, which is frequently used in image processing, has been applied to the magnetic anomaly map obtained in the Black Sea to determine the structure boundaries. They showed the sediments formed in the Black Sea on high resolution seismic sections [11]. They showed that the depressions formed in the Black Sea developed under periodically changing extreme pressure conditions driven by the North Anatolian Fault [12]. They interpreted with the help of seismic data that there is a compression tectonic regime that facilitates the migration of liquids to the seafloor in the Sorokin Trench in the Black Sea [13]. Gravity anomalies obtained in the Black Sea region were differentiated and compared with satellite data [14]. Using the gravity anomaly maps obtained in the Black Sea, they stated that the waters of the Caspian Sea could flow into the Black Sea through the Manych depression in the north of the Caucasus Mountains [15]. They applied the polarity reduction method to the magnetic anomaly map of the Black Sea region and took the Power Spectrum and calculated that the Curie point depths calculated in the Slovakia region were between 15.2 km and 20.9 km [16]. Using multi-beam bathymetric and multi-channel seismic reflection data obtained off the coast of Cide-Sinop, they revealed important records regarding the transgression of the Black Sea [17].

Materials and Methods: Cellular Neural Networks

Cellular neural networks are mostly composed of cells arranged in order to form a two-dimensional array. In contrast to known artificial neural networks, each cell is in close contact with cells in its immediate neighborhood (Figure-1). The basic function of the CNN method in image processing is to convert any input image into an output image according to the intended purpose. Here, when the output image is taken into account in the first form of the CNN method, each pixel value is limited to -1 and +1. However, the input images can have multiple gray levels after having the appropriate voltage values. After any transient initiated or driven by an input image, the CNN-treated image always converges to a steady-state fixed point if it meets the required conditions. In image processing, the CNN method is generally a non-linear and dynamic processing of a given input image to generate the output image.

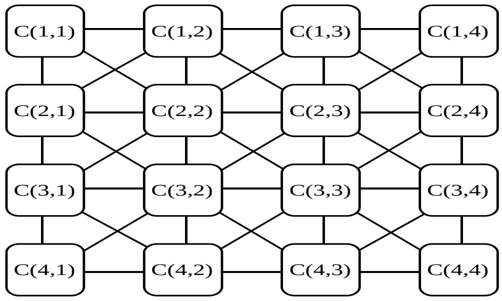

Figure 1: Two-dimensional (4x4) cellular neural network [9]

Each cell in these structures:

a) A linear input unit with a weighted aggregation

b) Linear dynamic interface

c) n It is a dynamic circuit consisting of an output unit (Piece-Wise Linear: PWL) according to the segmented (generally three-part) origin (Figure-2)

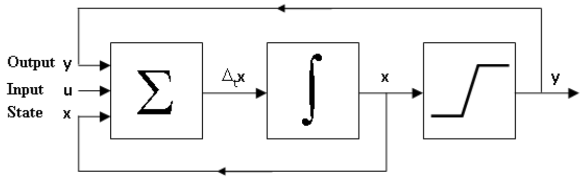

Figure 2: Block diagram of an artificial neural network [10]

The r-neighborhood of a cell in the Cellular Neural Network (CNN) is defined as follows.

$$N_r(i,j) = \{ C(k,l) \,|\, \max(|i-k|, |j-l|) \le r, \quad 1 \le \mathrm{i} \le \mathrm{M} ; 1 \le j \le \mathrm{N} \} \tag{1}$$

Here,

(i, j): The index vector, which determines the location of the cells in the array,

$C(i, j)$: i. line, j. is the parameter that represents the location of the cell in the column.

Differential equations that characterize the cellular neural network can be written as follows:

$$\frac{dx_{i,j}(t)}{dt} = -S \cdot x_{i,j}(t) + \sum_{(k,l)\in N(i,j)} A_{i,j;k,l} \cdot y_{k,l}(t) + \sum_{(k,l)\in N(i,j)} B_{i,j;k,l} \cdot u_{k,l}(t) + I_{i,j} \tag{2}$$

$$y_{i,j}(t) = f\left[x_{i,j}(t)\right] = \frac{1}{2} \cdot \left(\left| x_{i,j}(t) + 1 \right| - \left| x_{i,j}(t) - 1 \right| \right) \tag{3}$$

Burada:

$A_{i,j}$: feedback linkage coefficients

$B_{i,j}$: Input connection weight coefficients

I: The threshold level, which is usually the same for each cell

S: feedback weight coefficient is defined as.

The equation that characterizes the discrete time Cellular Neural Network is expressed as follows.

$$x_{i,j}(n+1) = \sum_{(k,l)\in N(i,j)} A_{i,j;k,l} \cdot y_{k,l}(n) + \sum_{(k,l)\in N(i,j)} B_{i,j;k,l} \cdot u_{k,l}(n) + I_{i,j} \tag{4}$$

$$y_{i,j}(n) = f\left[x_{i,j}(n)\right] = \frac{1}{2}\cdot\left(\left|x_{i,j}(n)+1\right| - \left|x_{i,j}(n)-1\right|\right) \quad (5)$$

In this equation, in addition to classical filtering, iterative filtering from feedback link weight coefficients A is also made.

Here, the inputs of the cells are real numbers with values in the range $u_{i,j}$, [-1,1]. The outputs $y_{i,j}$ of the cells are the outputs that can only have çıkış1 or +1 values if the stability conditions are reached at the end of a certain period (or cycle).

One of the most important features that distinguish CNN from artificial neural networks is that the feedback (A) and input (B) connection weight coefficients form a constant connection network on the studied plane (Space Invariance Property) (Figure 3).

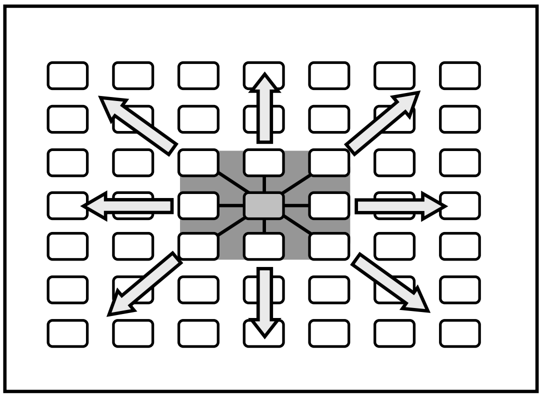

Figure 3: Invariance in plane [10]

$$A(i,j;k,l) = A(k-i,l-j) \qquad B(i,j;k,l) = B(k-i,l-j) \quad (6)$$

Results and Discussion: Field Application of the Method

The Black Sea is a large marginal sea located in the Alpine orogenic belt, bounded by compressed tectonic belts, the Pontides orogeny to the south, the Caucasus to the northeast, and the Crimean Region to the North [13]. It is located on the western side of the active Arabian-Eurasian collision and north of the North Anatolian Fault (NAF), which allows tectonic escape of Anatolia [18]. The Black Sea consists of two main expansion basins, the western and eastern Black Sea sub-basins (Figure 4). A complex NW-SE trending continental Central Black Sea Region is divided into two parts, the Andrussov Ridge in the north and the Archangelsky Ridge in the south [19].

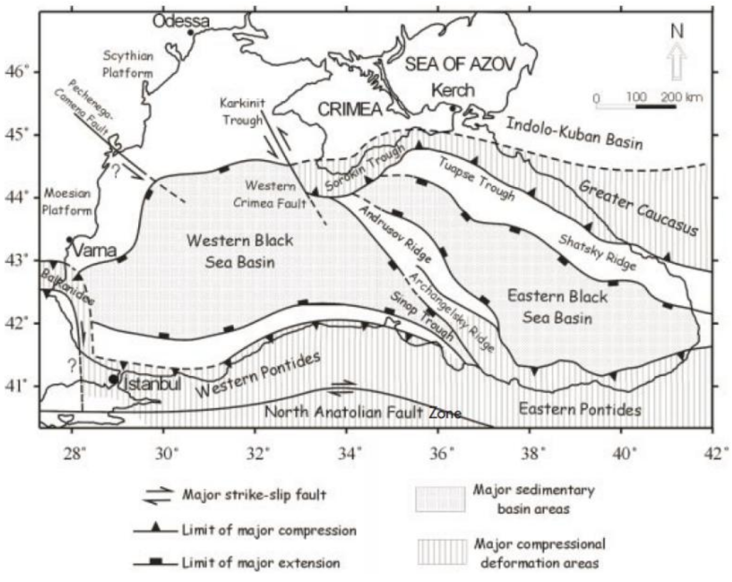

Figure 4: Karadeniz ve çevresindeki bölgenin genel tektonik yapısı [11, 19, 20]

The structure boundaries were tried to be found by applying the CNN method to the magnetic anomaly map of the Black Sea region (Figure 5a). The found structure boundaries were compared with the general tectonic structure of the Black Sea region given in Figure 4. The Eastern Black Sea basin undergoes a depression of about 12 km from the Early Tertiary [21]. This area is dominated by large extensional faults creating half-graben structures. The Archangelsky and Shatsky ridges represent regionally elevated foot blocks up to major extensional faults that form the southern and northern continental slopes of the region. However, the southern side of the basin was affected by the reactivate of widened faults and the development of new reverse faults at the end of the Eocene [22].

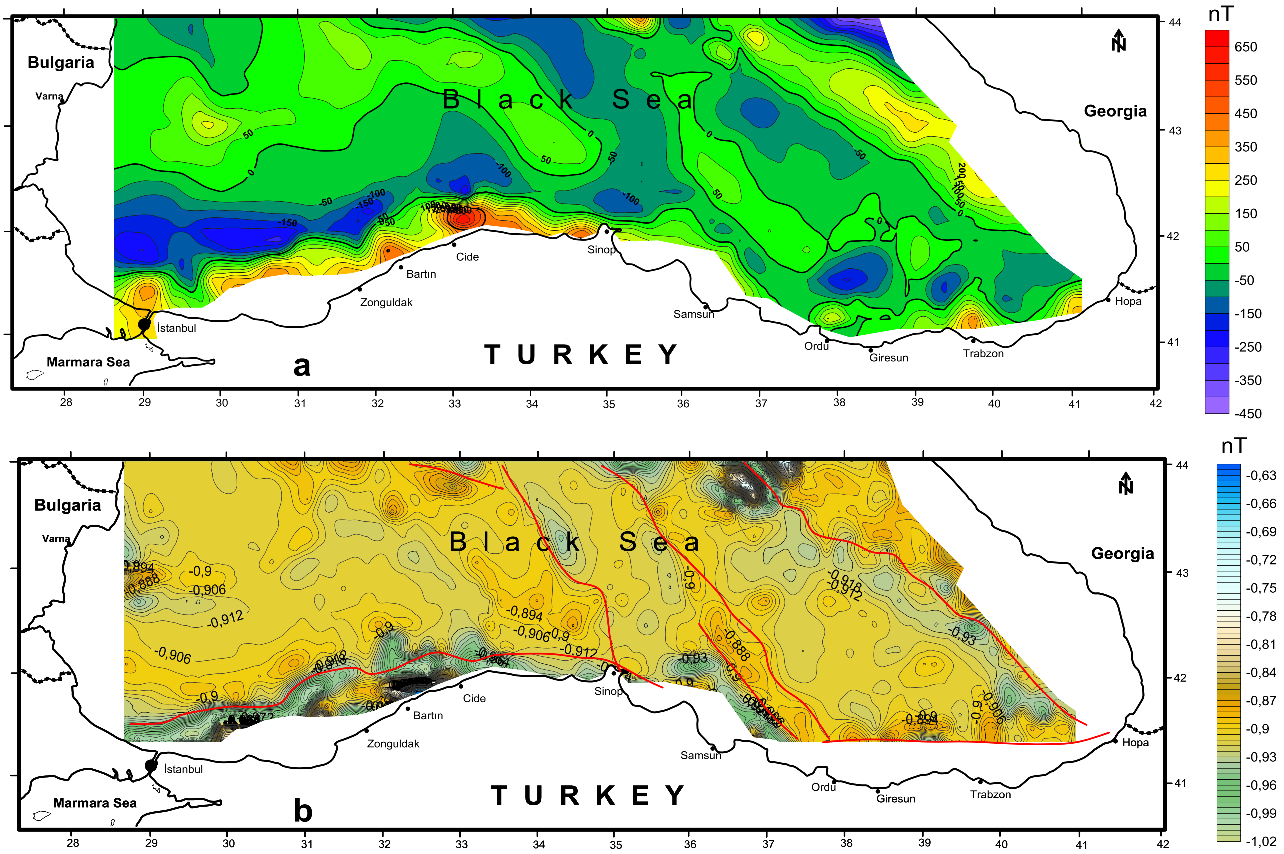

Figure 5: a) Magnetic anomaly map of the Black Sea (contour interval 50 nT) b) CNN output of the magnetic anomaly map (contour interval 0.006)

Conclusion

The Black Sea is a large marginal sea located in the Alpine orogenic belt, surrounded by compressed tectonic belts, the Pontides orogeny in the south, the Caucasus in the northeast, and the Crimea Region in the north (Fig. 4). The magnetic anomaly map taken by TPAO in the Black Sea region is given in figure 5a. The structure boundaries were determined by applying the CNN method to this magnetic anomaly map (Figure 5b). The locations of possible fault lines are determined by showing the building boundaries with red lines. When the structure boundaries are drawn and compared with the general tectonic structure of the Black Sea and its surroundings given in figure 4, it is seen that there is no complete harmony. Although the building boundaries given in Figure 4 are drawn slightly to the west, the boundaries we found with the magnetic data show more accurate locations. The Black Sea includes two main expansion basins, the western and eastern Black Sea sub-basins. This structure is separated by the NW-SE trending continental Central Black Sea Trench. It is divided into two as Andrussov Ridge in the north and Archangelsky Ridge in the south (Figure 4). The linearity of these two ridges is seen in the CNN output in Figure 5. The Archangelsky and Shatsky ridges are locally elevated to major extensional faults that form the southern and northern continental slopes of the region. However, the southern side of the basin has been affected by the reactivate of widened faults and the development of new reverse faults.

Acknowledgments

The authors wish to thank MTA for providing of magnetic potential field data for this study.

References

[1]. Chua L.O. and Yang L., 1998. Cellular Neural Networks: Theory, *IEEE Transactions on Circuits and Systems*, 35 (10), 1257 – 1272.

[2]. Matsumoto T., Chua L.O. and Yokohama T., 1990. Image Thinning with a Cellular Neural Network, *IEEE Transactions on Circuits and Systems*, 37 (5), 638–640.

[3]. Suzuki H., Matsimoto T. and Chua L.O., "A CNN Handwritten Character Recognizer", *International Journal of Circuit Theory and Applications*, 20: 601-612, 1992.

[4]. Slot K., 1992. Cellular Neural Network Design for Solving Specific Image-Processing Problems, *Internatinal Journal of Circuit Theory and Applications.* 20, 629-637.

[5]. Sziranyi T. and Csapodi M., "Texture Classification and Segmentation by Cellular Neural Network using Genetic Learning", *Research Report, Computer and Automation Institute Hungarian Academy of Sciences,* Budapest, Hungary, Kasım 1994.

[6]. Schultz A., 1998. Spatio Temporal CNN Algorithm for Object Segmentation and Object Recognition, *Fifth IEEE International Workshop on Cellular Neural Networks and Their Applications Proceedings,* South Bank University, London, UK, 347-352.

[7]. Özmen A., Uçan O.N. and Albora A.M., 1999. Arkeolojik Sahalarda Ölçülen Cisimlerin Hücresel Yapay Sinir Ağları Kullanılarak Görüntülenmesi, *TMMOB Jeofizik Mühendisleri Odası İzmir Şubesi-İZMİR*, 24.

[8]. Özmen A., Albora A.M. and Uçan O.N. 1999. Hücresel Yapay Sinir Ağları (HYSA) Kullanarak Sivas Bölgesi Gürün ilçesi Kötüyurttepe mevkiinin modellenmesi, *11.Mühendislik Haftası Yerbilimleri Sempozyumu*-ISPARTA, 373-381.

[9]. Albora A.M., Özmen A. ve Uçan O.N., 2001a. Residual Separation of Magnetic Fields Using a Cellular Neural Network Approach. *Pure and Applied Geophysics*, 158, 1797-1818.

[10]. Albora A.M., Uçan O.N., Özmen A. and Özkan T., 2001b. Separation of Bouguer anomaly map using cellular neural network, *Journal of Applied Geophysics*, 46, 129-142.

[11]. Çifci G., Dondurur D. and Ergün E., 2002. Sonar and High Resolution Seismic Studies in the Eastern Black Sea, *Turkish Journal of Earth Sciences*, 11, 61-81.

[12]. Çifci G., Dondurur D. and Ergün E., 2003. Deep and shallow structures of large pockmarks in the Turkish shelf, Eastern Black Sea, *Geo-Marine Letters*, 23, 311–322.

[13]. Krastel S., Spiess V., Ivanov M., Weinrebe W., Bohrmann G., Shashkin P., and Heidersdorf F. 2003. Acoustic investigations of mud volcanoes in the Sorokin Trough, Black Sea. *Geo-Marine Letters*., 23, 230-238.

[14]. Kılıçoğlu A. 2005. Gravıty anomaly map over the Black Sea using corrected sea surface heıghts from ers1, ers2 and Topex/Poseıdon Satellıte Altımetry Mıssıons. Stud. Geophys. Geod., 49.

[15]. Bahr A., Lamy F., Arz H. Kuhlmann H. and Wefer G. 2005. Late glacial to Holocene climate and sedimentation history in the NW Black Sea. *Marine Geology*, 214, 309– 322.

[16]. Rozimant K., Büyüksaraç A. And Bektaş O., 2009. Interpretation of Magnetic Anomalies and Estimation of Depth of Magnetic Crust in Slovakia. Pure appl. geophys. 166, 471–484.

[17]. Ocakoğlu N., İşcan Y., Kılıç Y., and Özel O., 2018. Morphologic and seismic evidence of rapid submergence offshore Cide-Sinop in the southern Black Sea shelf, *Geomorphology*, 311, 76-89.

[18]. Rangin C., Bader A.G, Pascal G., Ecevitoglu B., Görür N., 2002. Deep structure of the Mid Black Sea High (offshore Turkey) imaged by multi-channel seismic survey (BLACKSIS Cruise), *Mar Geol* 182, 265–278.

[19]. Robinson A.G., Rudat J.H., Banks C.J. and Wiles R.L.F., 1996. Petroleum geology of the Black Sea. Mar Petrol Geol 13,195–223.
[20]. Kazmin V.G., Schreider A.A. and Bulychev, A.A., 2000. Early stages of evolution of the Black Sea. In: Bozkurt, E., Winchester, J.A. and Piper, J.D.A. (eds) Tectonics and Magmatism in Turkey and the Surrounding Area. Geological Society, London, Special Publications 173, 235-249.
[21]. Finetti L., Bricchi G., Ben A.B., and Pipan M., 1998. Geopysical study of the Black Sea. Bollettino di Geofisica Teorica ed Applicata 30, 117,197-324.
[22]. Meredith D. and Egan S.S., 2002 The geological and geodynamic evolution of the Eastern Black Sea Basin: insights from 2-D and 3-D tectonic modeling. Tectonophysics 350(2):157-179.